33RD CONGRESS
OF THE INTERNATIONAL COUNCIL
OF THE AERONAUTICAL SCIENCES
STOCKHOLM, SWEDEN, 4-9 SEPTEMBER, 2022

ICAS 2022 SWEDEN

LATERAL GUST BEHAVIOUR OF AIRCRAFT INCORPORATING FLARED FOLDING WINGTIPS

R C M Cheung, H Gu, F Healy, D Rezgui & J E Cooper

Dept. of Aerospace Engineering, University of Bristol

Abstract

There has been much recent interest in new aircraft configurations to enable improved fuel efficiency. The concept of using flared folding wingtips (FFWT) to enable increased wing aspect ratios, whilst fitting airport gate restrictions, reducing gust / turbulence loads and improving roll performance, has shown encouraging results over the past 8 years. This paper considers a different loading case - the response of a flight mechanics aeroelastic model of a commercial aircraft with FFWT to a range of lateral "one minus cosine" gusts with different lengths. Comparisons are made between the locked and floating FFWT configuration responses and it is shown that the FFWT provides improved performance through alleviation of the deflections (and by implication the loads) but has little effect on the overall flight mechanics responses.

Keywords: flared folding wing tips, gust response, aeroelasticity, aircraft loads, sustainable aviation

1. Introduction

In recent years, there has been considerable research into the Floating Folding Wingtip (FFWT) concept, often referred to as the Semi-Aeroelastic Hinge (SAH) when referring to the situation when the wingtip is released on encountering a gust. This device allows the span of an aircraft to be reduced on the ground by folding the wingtips up on landing - allowing aircraft to operate using current airport infrastructure restrictions - whilst also having a larger span during flight and thereby reducing the induced drag. With regard to civil aircraft, currently such devices are only operated on the ground, such as on the Boeing 777x; however, its inclusion raises the question as to whether such a device could be utilised in-flight for aerodynamic or structural benefits.

One such device is the Flared Folding Wingtip (FFWT) [1–12] . As shown in Fig. 1, this device consists of a FWT in which the hinge line is rotated so that it is no longer parallel with the oncoming flow, with the magnitude of this rotation being defined as the flare angle, Λ. In this configuration an

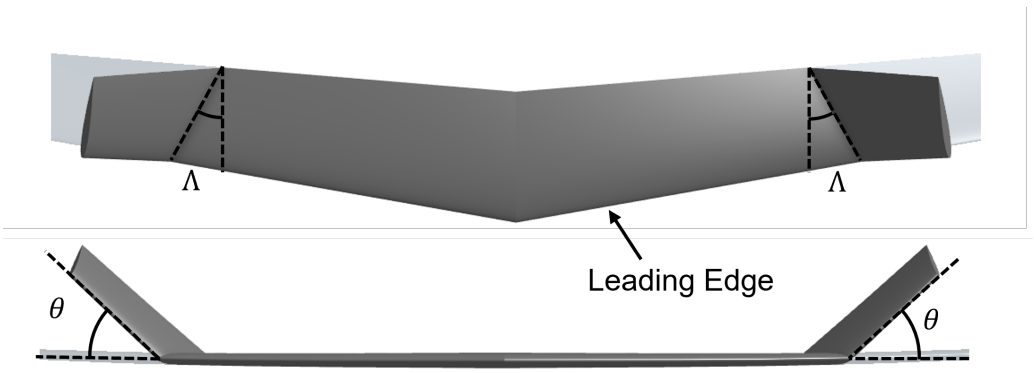

Figure 1 – Schematic of Floating Folding Wingtip

increase in the fold angle, θ , produces a decrease in the local Angle of Attack (AoA), and vice versa in the other direction. Therefore, when a FFWT is free to rotate, the fold angle tends to an equilibrium position, defined as the coast angle, about which the aerodynamic and gravitational moments balance, and the system is statically stable. Initial experimental and numerical research focused on the use of FFWTs as a passive gust alleviation device [1–6], as the large spanwise moment arm of a wingtip means such a device has a significant impact on the bending stresses seen along the entire wingspan. In the majority of these studies, absolute fold angles above 20 degrees are regularly seen. This geometric nonlinearity can significantly affect the overall system behaviour, with recent studies showing that accounting for this geometric nonlinearity can affect the load alleviation [13] and flutter speed [10] of a wing incorporating FFWTs.

Further research has focused on quantifying the effect of FFWTs on the handling qualities [8] and roll performance [9] of an aircraft, and flight tests have been conducted using the AlbatrossOne Unmanned Aerial Vehicle (UAV) [14, 15]. In particular, these flight tests showed that as the sideslip angle of the aircraft was varied, so did the equilibrium position of the wingtips, and at some critical sideslip angle the wingtips became unstable and folded on top of the inner wing. Furthermore, the coast angle and static stability of a FFWT was shown to be dependent on the flare angle [3]. As the flare angle increases the rate of change of aerodynamic forces on the wingtip with fold angle increases, reducing the required change in fold angle to achieve the same change in local AoA, and affecting its stability [3]. Similarly, as flare angle decreases, the rate of change of aerodynamic forces decreases and at a specific flare angle the rate of change of forces may change sign and the wingtip may become unstable. Conti et al. [16] numerically showed that, in terms of wingtip stability, changing the sideslip angle of an aircraft is equivalent to changing the flare angle of the FFWT, with the sideslip angle at which the wingtip becomes unstable being predicted as equal to the flare angle. However, flight tests with the AlbatrossOne UAV [15] found that the critical sideslip angle was significantly less than the flare angle of 17.5 degrees, with the wingtip becoming unstable and folding on-top of the inner wing at a sideslip angle of approximately 8-9 degrees, albeit there was a large amount of uncertainty in these measurements due to the dynamic nature of the flight test environment. The above findings may have significant implications for the handling qualities of an aircraft, as in flight conditions in which large sideslip angles could be achieved, such as in low speed manoeuvres and landing, the wingtips may either become unstable or fold over and collide with the inner wing, significantly changing the handling characteristic of an aircraft, potentially with catastrophic consequences.

This paper numerically explores a further important consideration for an aircraft incorporating the FFWT concept, the effect of lateral gusts on the aircraft behaviour. The response of a free-flying aircraft computational model with FFWTs to "1-cosine" lateral gusts is compared to the case where the wingtips are fixed. The findings from this work add to the current body of knowledge on the design of the FFWT concept.

2. Flight mechanics model

In this section, a flight mechanics model incorporating folding wingtips is described, including details on formulation of the underlying equation of motions. Figure 2 shows a schematic representation of the numerical model, with corresponding parameters listed in Table 1. In this numerical formulation, only wing flexibility is considered, while the fuselage and empennage are assumed rigid. Mass distribution of each wing is assumed uniform, with the elastic axis lying on the 50% chord position. Strip theory is used for computing the aerodynamic forces generated by the wings and the tail surfaces, with the aerodynamic axis located at the quarter-chord. The fuselage is assumed to generate zero lift. The wing motions are characterised using two elastic modes for the ease of formulation: first mode bending (quadratic bending deflection) and torsion (linear twist). The Lagrange equation is then employed to obtain the equations of motions in a second-order form. A similar approach is used to formulate the equations of motion of the folding wingtips, which are assumed to be rigid bodies. [17]

2.1 Wing motions

Bending displacement, Z_w, and torsional displacement, θ_w, of the wing can be expressed as

$$Z_w(x,y,t) = \left(\frac{y}{b}\right)^2 q_b(t) + \left(\frac{y}{b}\right)(x - x_f) q_t(t) \tag{1}$$

$$\theta_w(x,y,t) = (\frac{y}{s}) q_t(t) \tag{2}$$

where $q_b(t)$ and $q_t(t)$ are the corresponding generalised coordinate of wing bending and torsion respectively. $x - x_f$ is the chordwise distance between the bending and torsion axes. Therefore, the kinetic energy, T_{wing}, and the strain energy E_{wing} of the wing can be written as

$$T_{wing} = \frac{1}{2}\rho_m \int_0^b \int_{-0.5}^{0.5} [-(\frac{y}{b})^2 \dot{q}_b + (\frac{y}{b}) h c_h(y) \dot{q}_t]^2 dh dy \tag{3}$$

$$E_{wing} = \frac{1}{2}\int_0^b EI(\frac{2q_b}{b^2})^2 + GJ(\frac{q_t}{b})^2 dy \tag{4}$$

where h is the normalised distance between the elastic axes, and c_h is the local chord length at each spanwise position. A linear variation in local chord length with span, and therefore it may be formulated as

$$c_h(y) = C_0 - ky \tag{5}$$

where k is a constant determined by the taper ratio. The incremental work done by the aerodynamic forces is formulated as,

$$\delta Work_{wing} = \int_0^b -dL_W (\frac{y}{b})^2 \delta q_b + dM_W (\frac{y}{b}) \delta q_t \tag{6}$$

where dL_W represents the elemental lifting force acting on the wing, and M_W is the moment produced by the lift with respect to the wing elastic axis. For brevity, the derivation follows the starboard wing from hereon-in, while the contributions from the port wing can be derived using the same approach. Entities relating to the starboard wing is differentiated by the subscript R. Consider an elemental chordwise strip with length of c_h on the starboard wing panel, as shown in Figure 2, the lifting force can be expressed as

$$dL_{W,R} = Q_R a_w c_h(y) dy \alpha_{T,R} \tag{7}$$

Q_R is the local dynamic pressure. $\alpha_{T,R}$ is the effective angle of attack, which can be related to wing bending, $q_{b,R}$, torsion, $q_{t,R}$ and motions of centre of mass as

$$\alpha_{T.R} = \frac{W}{U} + \frac{W_g}{U} + \frac{y}{b} q_{t,R} \cos(\lambda) + \frac{y^2}{b^2}\frac{\dot{q}_{b,R}}{U} + \frac{2y\sin(\lambda) q_{b,R}}{b^2} + \frac{V\gamma}{U} + \frac{py}{U} \tag{8}$$

where W is the normal velocity, W_g is the vertical gust, V is the sideslip (lateral velocity) and p is the roll rate. The influence of yaw rate, r, on the aerodynamic forces on the wings is considered as a second order effect and it is therefore neglected in this study. The chordwise component of the velocity, U_c, on the strip can be related to the sweep angle, λ, and flight velocity, U, as

$$U_c = U\cos(\lambda) \tag{9}$$

In the presence of a sideslip angle, β, this component becomes

$$U_c = U\cos(\lambda - \beta) \tag{10}$$

and using the small angle approximation, the dynamic pressure on the local chord c_h, can be calculated as

$$Q_R = \frac{1}{2}\rho U^2(\cos(\lambda)^2 - 2\beta\cos(\lambda)\sin(\lambda)) \tag{11}$$

Since the aerodynamic centre (ac) of each strip is located at the quarter-chord, the elemental moment acting on the strip, $dM_{W,R}$, with respect to the elastic axis (x_f) is found as

$$dM_{W,R} = dL_{W,R}(0.25c_h) + Q_R C_m c_h^2 dy + Q_R c_h^2 M_{\dot{\theta}} \frac{y\dot{q}_t}{4bU} dy \tag{12}$$

where $M_{\dot{\theta}}$ represent the unsteady aerodynamic derivative which contributes to torsional damping [17]. By substituting Eq.(3),(4) and (6) into the Lagrange formulation, the wing motion can be expressed in the form

$$M \begin{Bmatrix} \ddot{q}_{b,R} \\ \ddot{q}_{t,R} \end{Bmatrix} + D \begin{Bmatrix} \dot{q}_{b,R} \\ \dot{q}_{t,R} \end{Bmatrix} + K \begin{Bmatrix} q_{b,R} \\ q_{t,R} \end{Bmatrix} = F_{Aero} \tag{13}$$

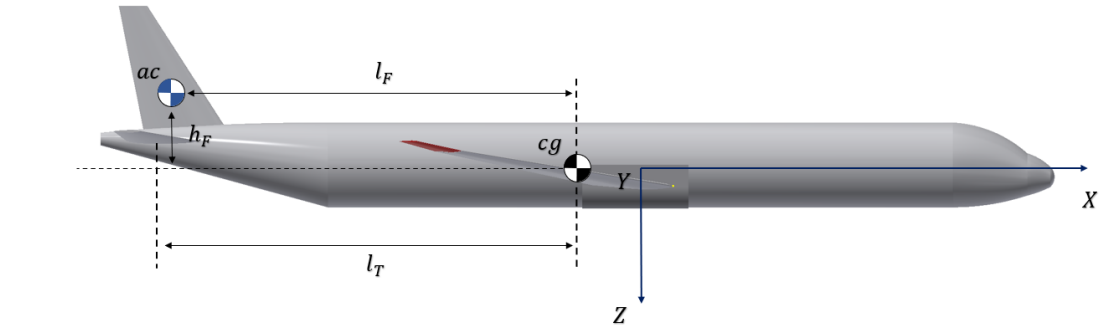

(a)

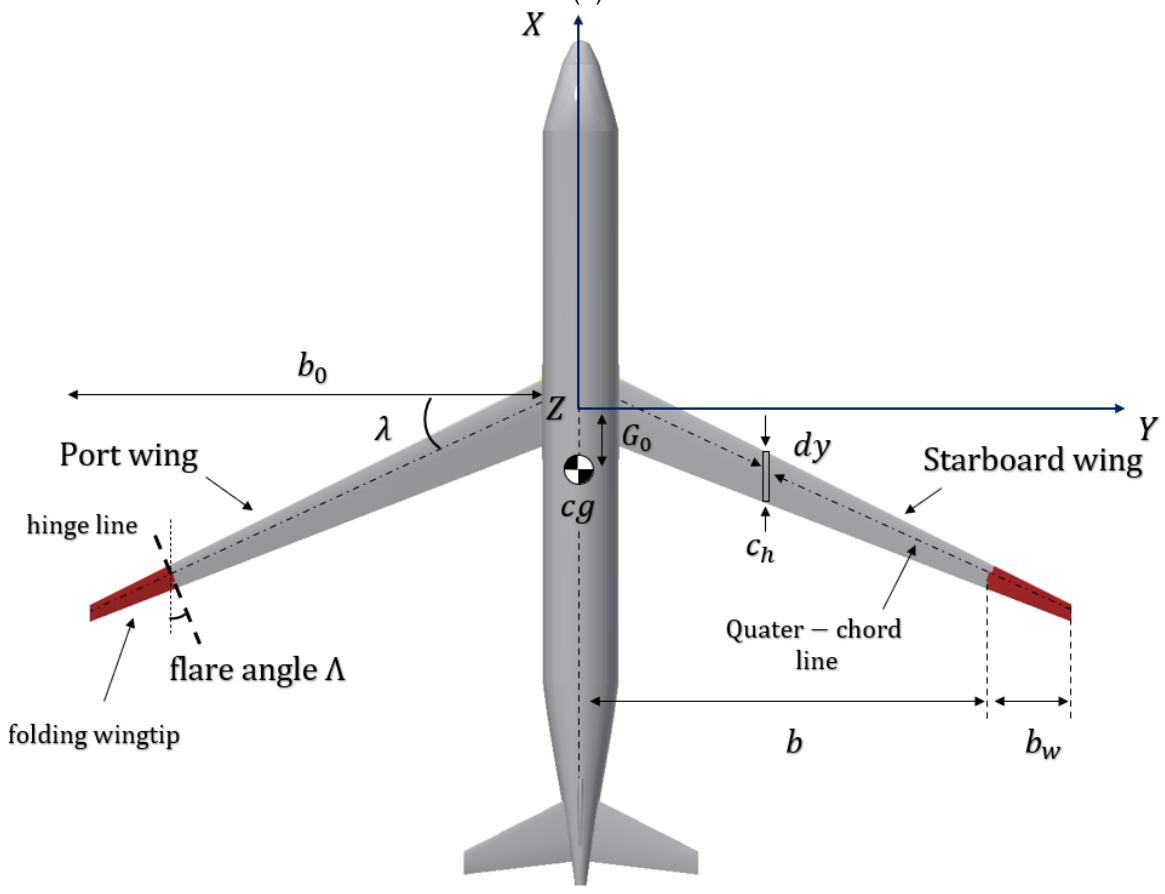

(b)

Figure 2 – Schematic drawing of an aircraft model incorporating folding wingtips. The coordinate system represents the body-axes with the origin located at the mid-chord position at the wing root.

2.2 Wingtip motion

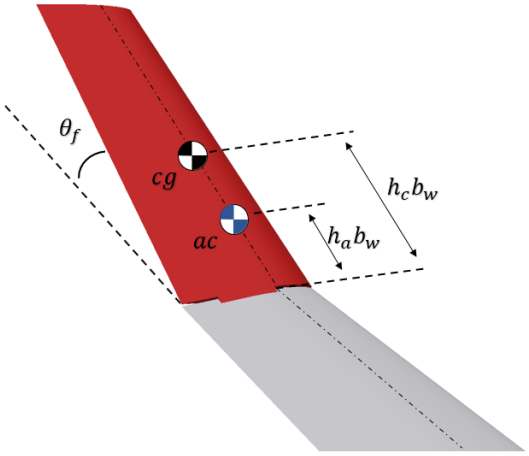

Figure 3 – Flared folding wingtip.

The folding wingtips are considered as rigid bodies and therefore the kinetic and potential energy relating to the wingtips become

$$T_{fwt} = \frac{1}{2} m_{fwt} (\dot{r_{fwt}})^T \cdot \dot{r_{fwt}} \tag{14}$$

$$U_{fwt} = m_{fwt} g \frac{\partial \vec{r_{fwt}}}{\partial z} \tag{15}$$

where $\vec{r_{fwt}}$ is the position vector of the centre of mass of the wingtip, cg, as shown in Figure 3. This vector refers to the position of the centre of mass, after accounting for the current folding angle, θ_f, as well as the deflection of the wing. Incremental work due to lift on the wingtip can be found as

$$\delta work_{fwt} = L_{fwt} \delta \vec{r_{ac}} \tag{16}$$

where $\vec{r_{ac}}$ is the position vector of the aerodynamic centre, ac, which is treated in the same way as $\vec{r_{fwt}}$ by considering the instantaneous folding angle of the wingtip and the deflection of the wing. L_{fwt} is the lift generated by the wingtip which is calculated using the same approach as the wing. By applying the Lagrangian approach to the expressions from Eq.(14) to (16), the equations of motion for the folding wingtips can be written in the form of a second order differential equation such that

$$M\ddot{\theta}_{fwt} + D\dot{\theta}_{fwt} + K\theta_{fwt} = F_{Aero} + A_{wing}(q_b, q_t, \dot{q}_b, \dot{q}_t, \ddot{q}_b, \ddot{q}_t) \tag{17}$$

where A_{wing} contains all the dependencies related to wing deflections. These equations are then combined with the wing motion equations and solved numerically as a single system.

2.3 Aircraft motion (six DOF model)

In this section, equations for the six degree-of-freedom motion of the aircraft are derived in the body axes using Newton's law. The generalised six degree of freedom equations of motion for a symmetric aircraft can be expressed as [18]

$$\begin{aligned}
m(\dot{U} - rV + qW) &= X \\
m(\dot{V} - pW + rU) &= Y \\
m(\dot{W} - qU + pV) &= Z \\
I_z\dot{p} - (I_y - I_z)qr - I_{xz}(pq + \dot{r}) &= L \\
I_y\dot{q} + (I_x - I_z)pr + I_{xz}(p^2 + r^2) &= M \\
I_y\dot{r} - (I_x - I_y)pq + I_{xz}(qr - \dot{p}) &= N
\end{aligned} \tag{18}$$

where X,Y,and Z are the axial, side and normal forces. p,q,and r are the roll, pitch and yaw rate. L,M,and N are the roll, pitch and yaw moment. The axial force, X, comprises of engine thrust, resultant lifting force, L_{all}, weight components and drag force may be expressed as

$$X = Thrust + L_{TL}\sin(\frac{W}{U}) - mg\sin(\theta) - \frac{1}{2}\rho U^2 S_W C_D \tag{19}$$

where L_{all} comprises of the lifting forces on the wings, L_W, and horizontal tail, L_T, and are written as

$$L_{TL} = -\int_0^b dL_{W,L} - \int_0^b dL_{W,R} - L_T - L_{fwt} \tag{20}$$

$$L_T = \frac{1}{2}\rho U^2 S_T(a_T(\frac{W}{U} + \frac{ql_T}{U} + \frac{W_g}{U}) + \eta\frac{dC_L}{d\eta}) \tag{21}$$

where S_T is the planform area of the horizontal tail, η is the elevator angle, and a_T is the lift-curve slope. For simplicity, the effect of sideslip has on the horizontal tail is neglected in this work. It is assumed that the side force, Y, is mainly caused by the vertical tail, drag of the fuselage and gravity. By substituting Eq. (19) into to Eq. (18), the side force equation can be obtained.

$$Y = mg\phi + \frac{1}{2}\rho U^2 S_F\left[a_F(-\frac{V}{U} + \frac{l_F r}{U}) + \zeta\frac{dC_L}{d\zeta}\right] - \frac{1}{2}\rho U^2 S_B\frac{V}{U}y_B \tag{22}$$

where S_F is the planform area of the vertical tail, S_B is the projected fuselage side area and ζ is the rudder deflection angle, and the term, $\frac{V}{U}y_B$ is equivalent to the lateral drag coefficient of the fuselage. The normal force Z (positive downwards), is determined through subtracting the lifting forces from the gravitational force such that

$$Z = mg\cos(\theta) - L_{all} \tag{23}$$

where the small angle approximation, $\cos(\theta) \approx 1$ is assumed. The roll moment, L, is predominantly caused by the vertical tail and the differential lift across the wingspan caused by aileron deflection and sideslip giving

$$L = \int_0^b y(dL_{W,L} - dL_{W,R}) + \int_{y_{a1}}^{y_{a2}} y(dL_{aW,L} - dL_{aW,R}) - \frac{1}{2}\rho U^2 S_F a_F\frac{V}{U}h_F \tag{24}$$

where h_F is the vertical distance between the aerodynamic centre of the vertical tail and the centre of mass of the aircraft. y_{a1}, and y_{a2} are the relative spanwise position of the aileron. $dL_{aW,L}$ and $dL_{aW,R}$ are the elementary lift on the port and starboard wing caused by the aileron deflections, which are expressed as

$$dL_{aW,L} = -Q_L c_h dy\frac{dC_L}{d\xi}\xi \tag{25}$$

$$dL_{aW,L} = Q_R c_h dy\frac{dC_L}{d\xi}\xi \tag{26}$$

The pitching moment, M, of the aircraft is predominantly contributed to by the lift on the wings and the empennage, thus

$$M = \int_0^b dL_{W,L}h_w + \int_0^b dL_{W,R}h_w + \frac{1}{2}\rho U^2 C_m\int_0^b c_h^2 dy - L_T l_T \tag{27}$$

where h_w is the distance between aerodynamic centre of each strip and centre of mass of the aircraft which varies linearly along the wingspan as a function of the sweep angle, λ

$$h_w = G_0 + 0.25C_0 - y\tan(\lambda) \tag{28}$$

G_0 is the centre of mass position of the aircraft relative to the origin of the body axis shown in Figure 2 (b). The yaw moment, N, is mainly provided by the vertical tail, and can be calculated through the expression

$$N = -\frac{1}{2}\rho U^2 S_F l_F \left[\left(\frac{l_F r}{U} - \frac{V}{U}\right)a_F + \frac{dC_L}{d\zeta}\zeta\right] \tag{29}$$

The six degree of freedom equations of motion are then obtained by substituting Eq. (19),(22), (23) (24),(27), (29) into Eq. (18).

Table 1 – Summary of the aircraft configuration.

Aircraft geometric parameters	**Value**
Wingspan (b_0)	31.0m
Wing planform area (S_W)	122.4 m^2
Taper ratio	0.24
Aspect ratio (AR)	9.39
Horizontal tail planform area (S_T)	31.0 m^2
Vertical tail planform area (S_V)	21.5 m^2
Wing sweep (λ)	25.0°
Wing dihedral (γ)	5.0°
Wing initial setting angle (α_0)	4.0°
Horizontal tail initial setting angle (i)	-2.0°
Aileron position(y_{a1} to y_{a2})	0.7b to 0.9b
Horizontal tail moment arm (l_T)	13.53m
Vertical tail moment arm (l_F)	12.53m
centre of mass position (G_0)	25% MAC
Folding wingtip flare angle(Λ)	15°
Mass configurations	
Aircraft mass (m)	50000 kg
Wing density (ρ_m)	60 kg/m^2
Roll inertia (I_x)	1.267×10^6 kg.m^2
Pitch inertia (I_y)	2.441×10^6 kg.m^2
Yaw inertia (I_z)	3.925×10^6 kg.m^2
Aerodynamic characteristics	
Wing lift-curve slope (a_W)	5.5 /rad
Horizontal tail lift-curve slope (a_T)	3.9 /rad
Vertical tail lift-curve slope (a_F)	2.5 /rad
Elevator lift-curve slope ($\frac{dC_L}{d\eta}$)	1.5 /rad
Aileron lift-curve slope ($\frac{dC_L}{d\xi}$)	0.4 /rad
Rudder lift-curve slope ($\frac{dC_L}{d\zeta}$)	0.85 /rad
Moment coefficient of the wing (C_m)	-0.1
Flight case	
Altitude	36000 ft
March number	0.78
Air density	0.4 kg/m^3
Trim drag coefficient (C_D)	0.036

3. Lateral Gust Response Behaviour

The flight mechanics numerical model was trimmed to the flight condition specified in Table 1, corresponding to 220m/s airspeed, which gives a coast angle at cruise of 16.6°. A wide range of parameters for the overall aircraft behaviour and also the wing and wing-tip deflections were computed for lateral gusts, from the starboard side, of lengths between 20m and 220m as per the EASA airworthiness regulations. Both floating and fixed wing tip conditions were considered. Figures 4 to 10 show typical responses for the 100m gust length of the following interesting quantities:

- Port Wing bending at hinge
- Starboard Wing bending at hinge
- Port Wing FWT angle
- Starboard Wing FWT angle
- Aircraft Roll angle
- Aircraft Pitch angle
- Aircraft Yaw angle

It can be seen that there is a rapid damped oscillation for the wing bending deflections and fold angles corresponding primarily to the first wing bending mode, whereas the aircraft roll, pitch and yaw motions are of a much lower frequency, relating to the aircraft dynamic modes.

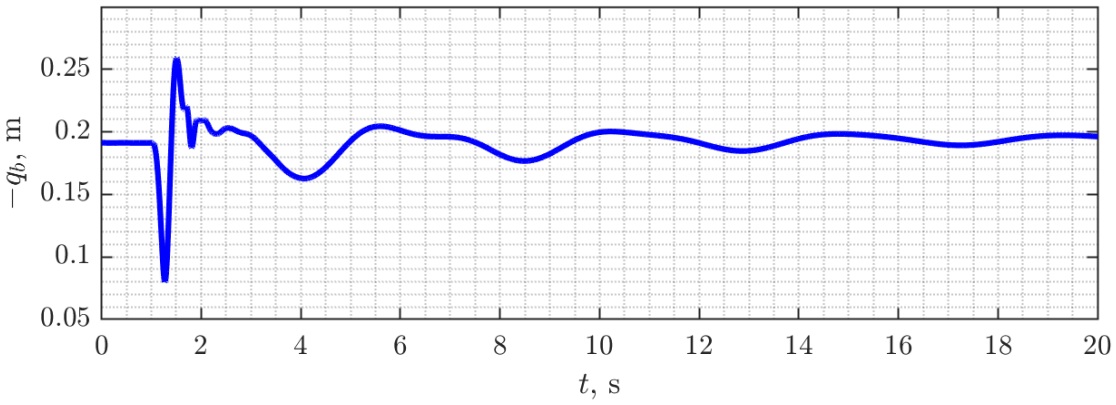

Figure 4 – Port Wing bending at hinge from 100m Lateral Gust.

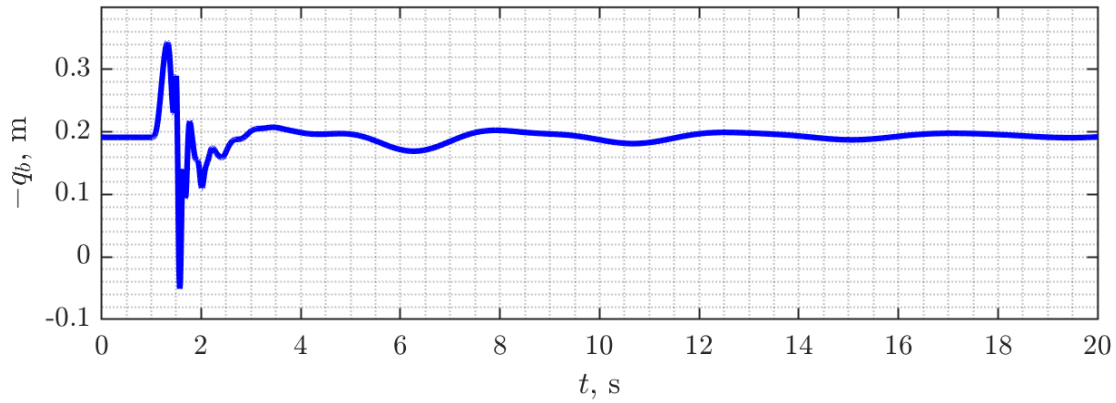

Figure 5 – Starboard Wing bending at hinge from 100m Lateral Gust.

Considering the wingtip hinge motion and corresponding wing bending deflections at the hinge through the duration of the gust, Figure 11 shows how the starboard wingtip rotates upwards (decrease in lift) whereas the initial motion of the port wingtip is a downward rotation (increase in lift). At a first glance the bending motion, shown in Figure 12 of the two wings is contrary to what might be expected, as the starboard wing initially deflects in upward direction while the port wing bends down. In general, the fixed case wing deflections are greater than those of the floating wingtip case. However, it is worth mention that the aircraft is incorporated with swept-back wings, where the presence of the sweep angle will overcome those of the FFWTs. Following the initial deflections there are some

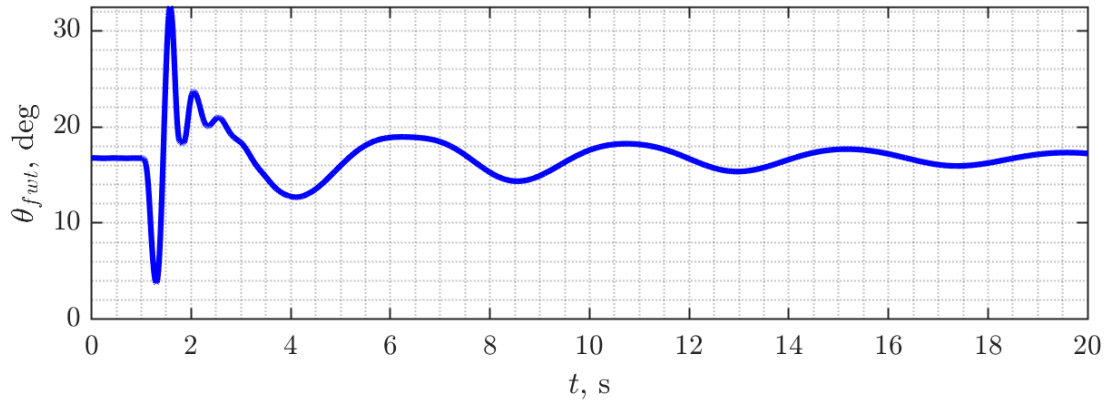

Figure 6 – Fold angle of port folding wingtip from 100m Lateral Gust.

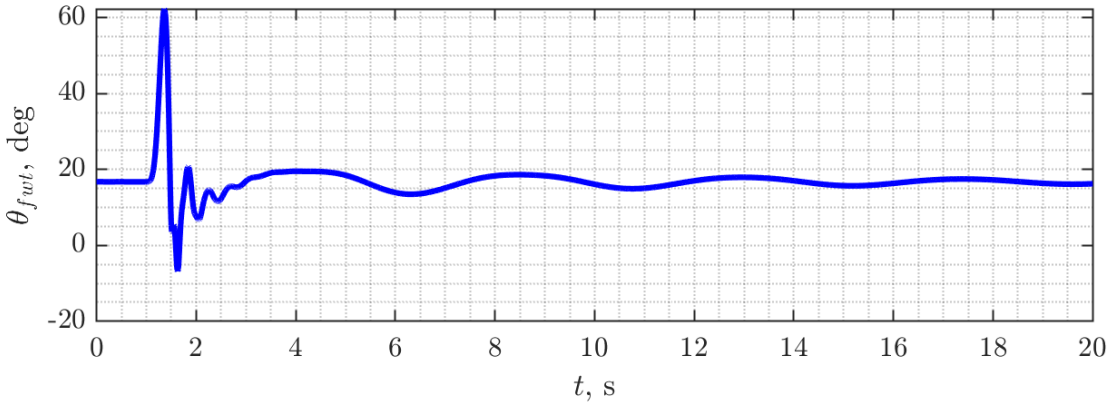

Figure 7 – Fold angle of starboard folding wingtip from 100m Lateral Gust.

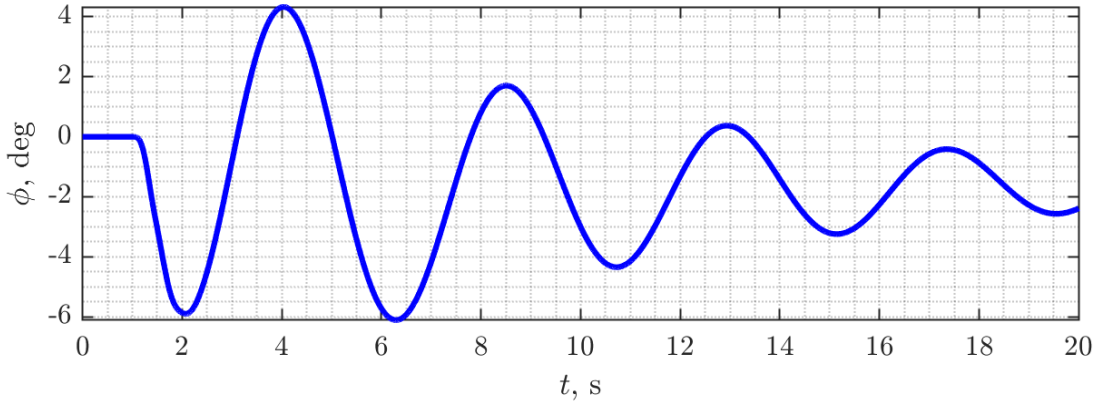

Figure 8 – Aircraft roll angle from 100m Lateral Gust.

damped oscillations before returning to the trim condition.

Figure 13 considers the effect of gust length on the FWT hinge fold rotations. For the locked hinge case, the rotations are zero by definition. When the hinges are unlocked, the starboard wing hinge rotations are much greater than those of the port wing, as the lateral gust pushes the starboard wingtip to larger deflections. Beyond a gust length of 60m the minimum starboard wingtip rotation is negative.

Figure 14 shows the maximum and minimum, port and starboard, wing bending deflections for the floating and locked wingtip cases undergoing varying gust length excitation. It can be seen that the

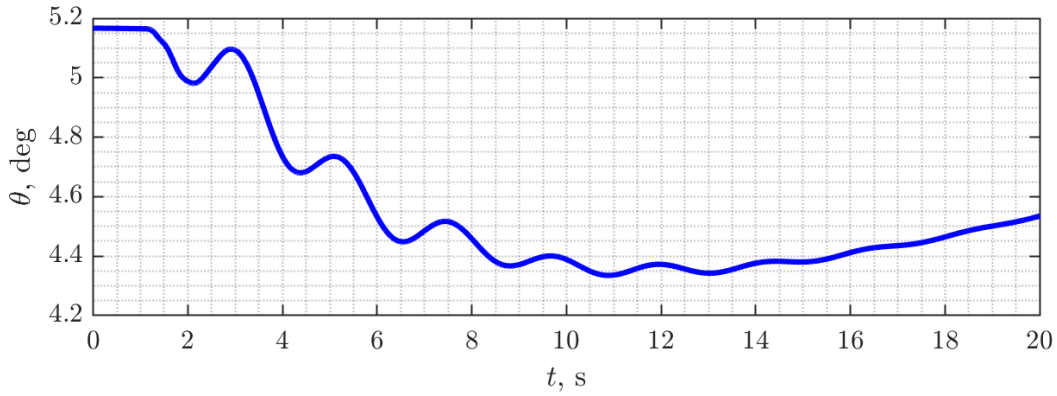

Figure 9 – Aircraft pitch angle from 100m Lateral Gust.

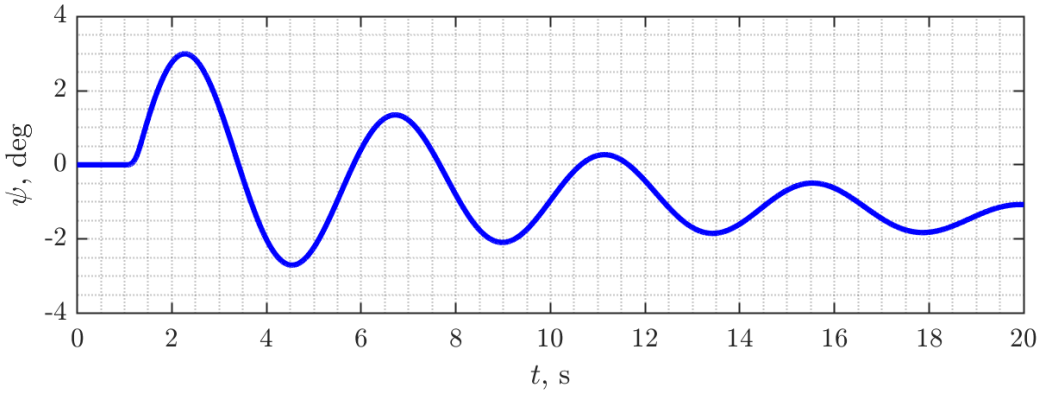

Figure 10 – Aircraft yaw angle from 100m Lateral Gust.

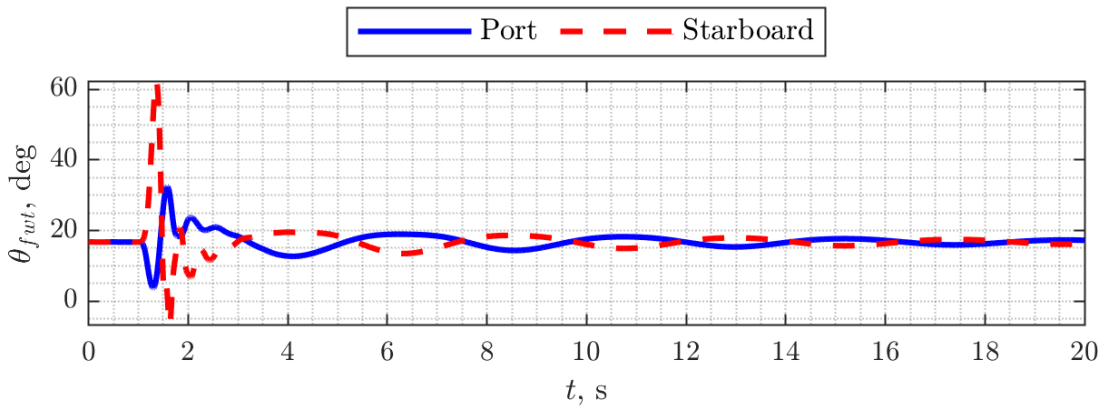

Figure 11 – Folding wingtip hinge angle response.

maximum wing bending is generally higher for the starboard wing when the wingtips are locked, but not by a great deal. This effect is due to the backward sweep and dihedral of the wings enabling the starboard wing to gain higher lift. When the wingtips are unlocked, the starboard wing still deflects more than the port wing; however, the rotation of the floating wingtips, as shown previously in Figure 13, reduces the total lift gain and thus results in lower bending deflections when compared with the locked case. This reduction in deflection also implies that the resultant bending moments along the wing are lower.

Figure 15 shows the comparison between the locked and floating wingtip cases for maximum and minimum roll, yaw and pitch motions with respect to lateral gust length. It can be seen that the range of roll and yaw motion is similar between the two wingtip cases. For the pitch motion, the range of

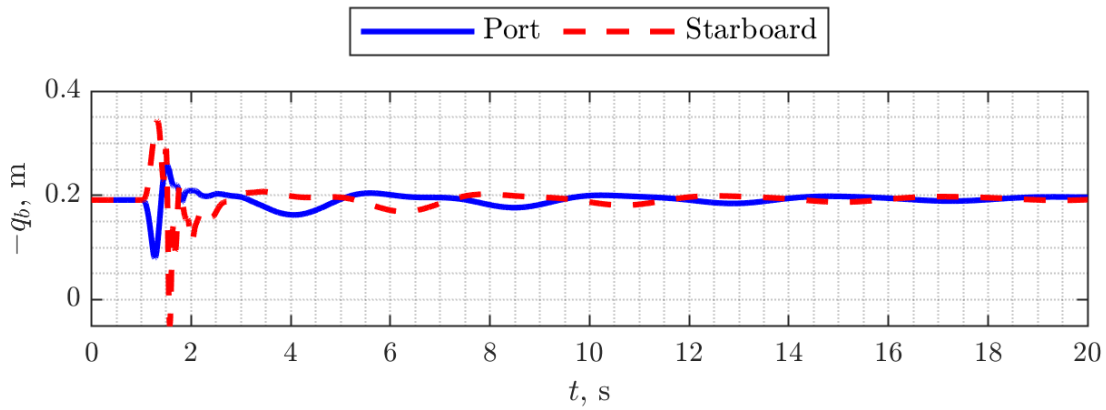

(a) FWT floating.

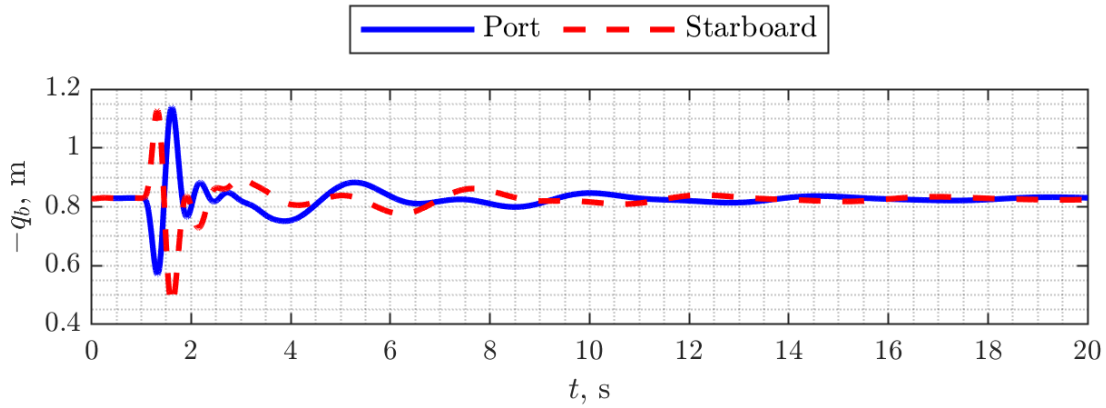

(b) FWT locked.

Figure 12 – Wing bending response from 100m Lateral Gust.

motion is marginally reduced when the wingtips are floating. These initial results indicate that the flared folding wingtips will only cause a negligible impact on the overall aircraft dynamics.

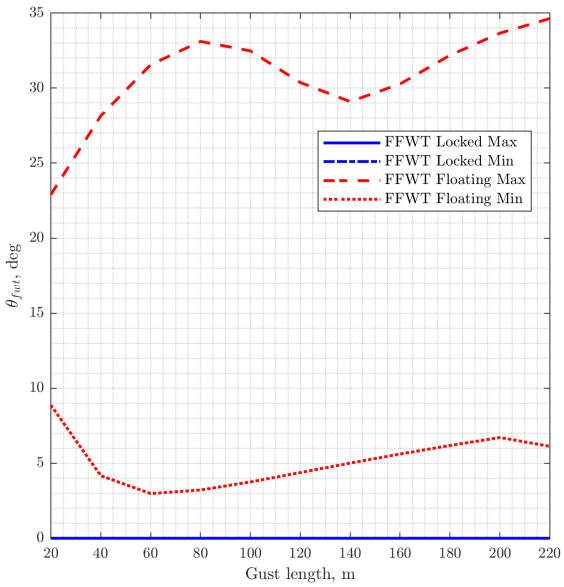

(a) Port wing.

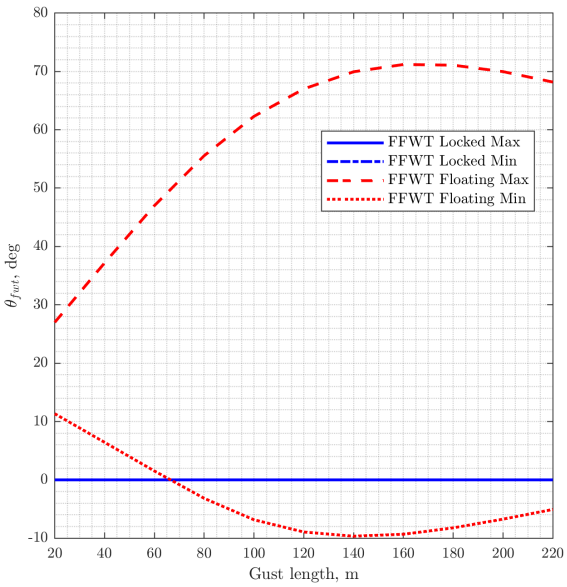

(b) Starboard wing.

Figure 13 – Max & Min Wingtip fold angle with respect to gust length.

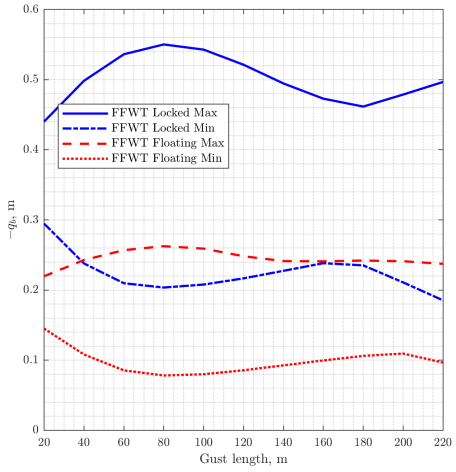

(a) Port wing.

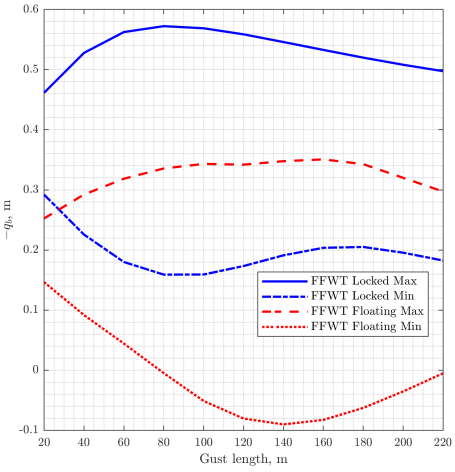

(b) Starboard wing.

Figure 14 – Max & Min Wing bending response with respect to gust length.

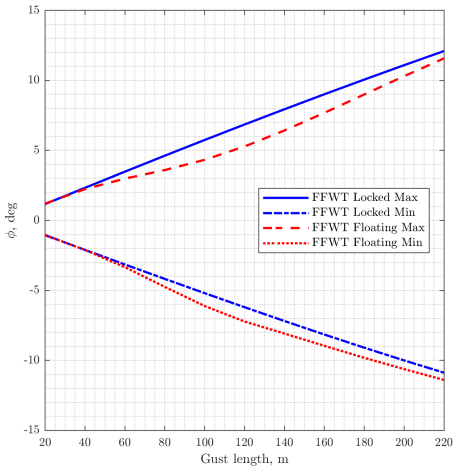

(a) Roll Angle

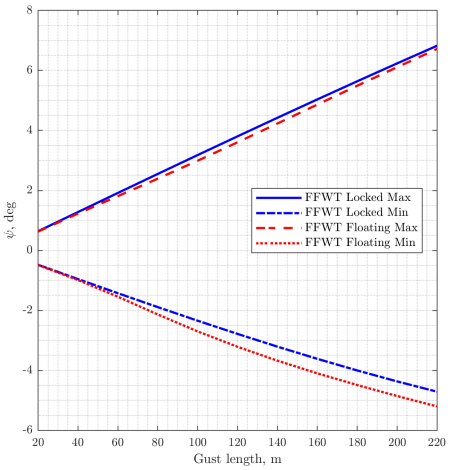

(b) Yaw Angle

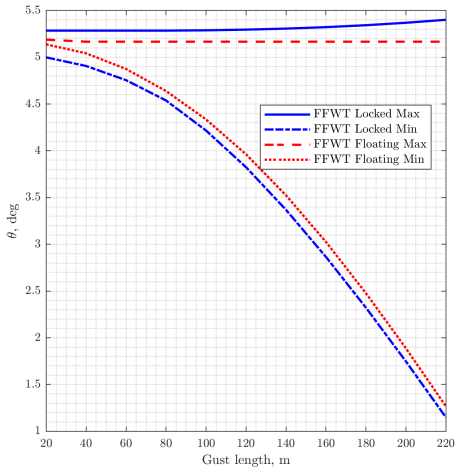

(c) Pitch Angle

Figure 15 – floating and Locked Aircraft: a) roll angle, b) yaw angle and c) pitch angle, response with respect to gust length.

4. Conclusions

This paper present a study into the effect of lateral gusts on the flight behaviour of an aircraft incorporating the Flared Folding Wing Tip concept. A numerical flight mechanics aircraft model was developed and used to explore the response to a family of different length lateral "one minus cosine" gusts when floating folding wingtips were implemented . These results were compared to the case where the folding wing tips were fixed. It was found that whereas the folding wingtips were beneficial in terms of reducing the wing bending deflections (and by implication the bending moments) they had little effect on the overall aircraft flight mechanics behaviour during a lateral gust encounter.

5. Acknowledgments

This work has received financial support from the UK Aerospace Technology Institute DAWS and XWING-ALPHA projects, and also via an Engineering and Physical Science Research Council iCASE award (19000004) sponsored by Airbus Operations UK Ltd.

6. Copyright Statement

7. Contact Author Email Address

mailto: r.c.m.cheung@bristol.ac.uk

References

[1] Ronald C. M. Cheung, Djamel Rezgui, Jonathan E. Cooper, and Thomas Wilson. Testing of a hinged wingtip device for gust loads alleviation. *Journal of Aircraft*, 55(5):2050–2067, 2018.

[2] R. C. M. Cheung, D. Rezgui, J. E. Cooper, and T. Wilson. Testing of folding wingtip for gust load alleviation of flexible high-aspect-ratio wing. *Journal of Aircraft*, pages 1–13, 2020.

[3] A. Castrichini, V. Hodigere Siddaramaiah, D. E. Calderon, J. E. Cooper, T. Wilson, and Y. Lemmens. Preliminary investigation of use of flexible folding wing tips for static and dynamic load alleviation. *The Aeronautical Journal*, 121(1235):73–94, 2017.

[4] A. Castrichini, V. Hodigere Siddaramaiah, D. E. Calderon, J. E. Cooper, T. Wilson, and Y. Lemmens. Nonlinear folding wing tips for gust loads alleviation. *Journal of Aircraft*, 53(5):1391–1399, 2016.

[5] Davide Balatti, Hamed Haddad Khodaparast, Michael I. Friswell, Marinos Manolesos, and Mohammadreza Amoozgar. The effect of folding wingtips on the worst-case gust loads of a simplified aircraft model. *Proceedings of the Institution of Mechanical Engineers, Part G: Journal of Aerospace Engineering*, 2021.

[6] Gaétan Dussart, Sezsy Yusuf, and Mudassir Lone. Identification of in-flight wingtip folding effects on the roll characteristics of a flexible aircraft. *Aerospace*, 6(6):63, 2019.

[7] Thomas Wilson, Andrea Castrichini, Alvaro Azabal, Je Cooper, Rafic Ajaj, and Martin Herring. Aeroelastic behaviour of hinged wing tips. In *International Forum of Aeroelasticity and Structural Dynamics*, Como, Italy, 2017.

[8] Andrea Castrichini, Thomas Wilson, Francesco Saltari, Franco Mastroddi, N. Viceconti, and J. Cooper. Aeroelastics flight dynamics coupling effects of the semi-aeroelastic hinge device. *Journal of Aircraft*, pages 1–9, 2019.

[9] Fintan Healy, Ronald Cheung, Theodor Neofet, Mark Lowenberg, Djamel Rezgui, Jonathan Cooper, Andrea Castrichini, and Tom Wilson. Folding wingtips for improved roll performance. *Journal of Aircraft*, pages 1–14, 2021.

[10] Fintan Healy, Ronald C. Cheung, Djamel Rezgui, Jonathan E. Cooper, Thomas Wilson, and Andrea Castrichini. On the nonlinear geometric behaviour of flared folding wingtips. In *AIAA SCITECH 2022 Forum*, 2022.

[11] Mark Drela. Development of the d8 transport configuration. In *29th AIAA Applied Aerodynamics Conference*, Honolulu, Hawaii, 2011.

[12] Huaiyuan Gu, Fintan Healy, and Jonathan E. Cooper. Sizing of high aspect ratio wings incorporating folding wingtip. In *AeroBest*, Lisbon, Portugal, 2021.

[13] Divya Sanghi, Cristina Riso, Carlos E. Cesnik, and Fabio Vetrano. Conventional and unconventional control effectors for load alleviation in high-aspect-ratio-wing aircraft. In *AIAA SCITECH 2022 Forum*, 2022.

[14] Thomas Wilson, James Kirk, John Hobday, and Andrea Castrichini. Small scale flying demonstration of semi aeroelastic hinged wing tips. In *International Forum on Aeroelasticity and Structural Dynamics*, Savannah, Georgia, USA, 2019.

[15] Fintan Healy, Alessandro Pontillo, Djamel Rezgui, Jonathan E. Cooper, James Kirk, Thomas Wilson, and Andrea Castrichini. Experimental analysis of the dynamics of flared folding wingtips via a novel tethered flight test. In *AIAA Scitech 2022 Forum*, 2021.

[16] Claudio Conti, Francesco Saltari, Franco Mastroddi, Thomas Wilson, and Andrea Castrichini. Quasi-steady aeroelastic analysis of the semi-aeroelastic hinge including geometric nonlinearities. *Journal of Aircraft*, pages 1–11, 2021.

[17] Jan Wright and Jonathan E. Cooper. *Introduction to Aircraft Aeroelasticity and Loads*. Aerospace Series. Wiley, Chichester UK, 2015.

[18] Michael Cook. *Flight Dynamics Principles: A Linear Systems Approach to Aircraft Stability and Control*. Butterworth-Heinemann, 3^{rd} edition, 2012.